

# Digenite ( $\text{Cu}_9\text{S}_5$ ): Layered p-Type Semiconductor Grown by Reactive Annealing of Copper

Anat Itzhak,<sup>†,||</sup> Eti Teblum,<sup>†,||</sup> Olga Girshevitz,<sup>‡</sup> Sivan Okashy,<sup>†</sup> Yury Turkulets,<sup>§</sup> Luba Burlaka,<sup>‡</sup> Gili Cohen-Taguri,<sup>‡</sup> Efrat Shawat Avraham,<sup>†</sup> Malachi Noked,<sup>†</sup> Ilan Shalish,<sup>\*,§,||</sup> and Gilbert Daniel Nessim<sup>\*,†,||</sup>

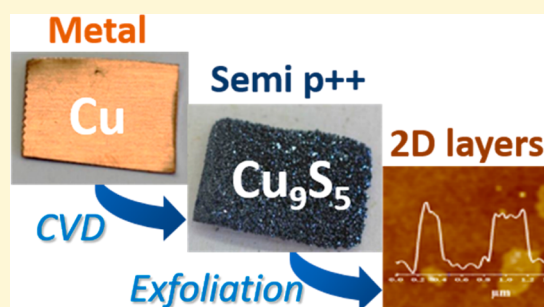
<sup>†</sup>The Department of Chemistry and Institute of Nanotechnology, Bar-Ilan University, Ramat Gan 52900, Israel

<sup>‡</sup>Institute of Nanotechnology & Advanced Materials, Bar-Ilan University, Ramat Gan 52900, Israel

<sup>§</sup>Department of Electrical and Computer Engineering, Ben Gurion University of the Negev, Beer Sheva 8410501, Israel

## Supporting Information

**ABSTRACT:** Most of the recently discovered layered materials such as  $\text{MoS}_2$  or  $\text{MoSe}_2$  are n-type, while few materials, such as phosphorene, which suffers from rapid oxidation, are p-type. To form devices such as p–n junctions and heterojunctions, new p-type mono-/few-layers are needed. Here, we report a one-step synthesis of layered, crystalline, p-type copper sulfide by thermal annealing of a standard copper foil in an inert environment using chemical vapor deposition (CVD). Optical spectroscopies (photoluminescence and absorption) show definite correlating features around 2.5 eV. Surface photovoltage spectroscopy shows a photovoltage reduction around the same energy range, which would be expected from a bandgap of a p-type material, and p-type conductivity was also observed using a thermoelectric probe. TEM, XRD, and AFM showed that the synthesized material is layered and has a unique stoichiometry of  $\text{Cu}_9\text{S}_5$ . Using sonication and dropcasting, we succeeded to isolate few-layers and monolayers. We observed good bulk electrical conductivity and characterized the electrical conductivity of few-layer copper sulfide flakes using peak force tunneling atomic force microscopy (PF-TUNA). We observed an increase in conductivity for increasing number of layers. Given its conductivity and layered morphology, we tested the synthesized  $\text{Cu}_9\text{S}_5$  as an electrode for a Li-ion battery. The proposed bottom-up synthesis, which is simple and scalable, allows synthesizing bulk quantities of the p-type layered  $\text{Cu}_9\text{S}_5$  which can then be exfoliated (top-down) to deposit monolayer flakes on substrates. Combined with the progress achieved in the preparation of n-type layered materials, this p-type  $\text{Cu}_9\text{S}_5$  opens the door to the fabrication of 2D p–n heterojunctions.



## INTRODUCTION

Over a decade ago, it was demonstrated that graphene can be easily exfoliated from a graphite crystal.<sup>1–3</sup> This method gave rise to a surge of basic and applied research on graphene, which exhibits exotic properties that greatly differ from its 3D version, graphite.<sup>4</sup> In spite of the progress made in the study of graphene, its use in electronics and photonics is still limited and is facing several barriers, the most important being the absence of an energy bandgap.<sup>5</sup> Attempts have been made to open a bandgap wide enough in graphene to make it useful, but they resulted in a loss of its exotic properties.<sup>6</sup>

As a result, the attention has shifted to other layered crystalline materials, which have been investigated over decades.<sup>7–9</sup> These materials are composed of planes of covalently bonded atomic layers, ranging from one to several atoms thick, which are weakly bonded to each other by van der Waals forces. For all layered materials, research in recent years has shown that, in addition to composition and atomic structure, dimension plays a pivotal role in defining material properties, especially the bandgap.<sup>10–13</sup>

A popular class of the known lamellar materials are transition metal dichalcogenides (TMDs), compounds of a group VI element with a transition metal.<sup>12,13</sup> Recently, these materials have received much attention for having a variety of unique physical properties and for covering a wide range of bandgaps.<sup>9,14,15</sup> While graphene is a semimetal, TMDs often exhibit high mobility<sup>16,17</sup> and span a wider selection of conduction properties: insulators, semiconductors, and semi-metals.<sup>18</sup> In most cases, their bandgap is direct for monolayers<sup>19–21</sup> and indirect for two or more layers. This makes TMDs suitable for many applications, including thin, flexible devices;<sup>22</sup> optoelectronic devices;<sup>23–25</sup> transistors;<sup>16,26,27</sup> lithium-ion batteries;<sup>28</sup> lubrication;<sup>29</sup> and catalysis.<sup>30</sup> Monolayers of  $\text{MoS}_2$ ,  $\text{WS}_2$ , and  $\text{VS}_2$  can be fabricated using bottom-up synthesis such as chemical vapor deposition (CVD),<sup>31–34</sup> or top-down using different methods such as

Received: January 15, 2018

Revised: March 6, 2018

Published: March 12, 2018

mechanical exfoliation,<sup>35,36</sup> liquid exfoliation,<sup>37,38</sup> or lithium intercalation/deintercalation<sup>39</sup> from their bulk materials. Among them, CVD appears to be the most promising method, especially for device applications, due to its industrial scalability and the good quality obtained to date in synthesizing many TMDs, including direct growth of monolayers on substrates.<sup>40,41</sup>

Focusing on device applications, the vast majority of layered semiconducting materials (including TMDs) are n-type because the most frequent defect in compound semiconductors is an anion vacancy.<sup>42</sup> However, to form p–n junctions or heterojunctions, one also needs p-type materials. The recently synthesized phosphorene is the most popular and versatile layered p-type material, but suffers extensively from oxidation.<sup>43</sup> Besides phosphorene, there have been several suggestions to obtain p-type conductivity in n-type TMDs by doping of MoS<sub>2</sub>, e.g., using contact-induced conductivity<sup>44</sup> or phosphorus implantation.<sup>45</sup>

Copper sulfides (with a formula of Cu<sub>2–x</sub>S, with  $x \leq 1$ ) have been extensively researched.<sup>46,47</sup> They are intrinsic hole-conducting (p-type) semiconductors,<sup>42</sup> and usually they exhibit a direct bandgap ranging from 1.2 to 2.5 eV,<sup>46</sup> depending on the specific phase and stoichiometry.<sup>48</sup> It was shown that the bandgap can be tuned by varying the concentration of Cu vacancies.<sup>48</sup> Cu<sub>2–x</sub>S is a low-cost, environmentally benign, nontoxic material.<sup>49</sup> Due to its excellent thermoelectric properties,<sup>50,51</sup> it is considered a promising candidate for various applications such as cathodes of lithium-ion batteries,<sup>52–54</sup> solar cell absorbers,<sup>55,56</sup> sensors,<sup>57–59</sup> and various optoelectronic devices.<sup>60,61</sup>

Over the past decade, numerous approaches have been developed to synthesize copper sulfides in various morphologies, spatial orientations, and shapes, which were found to affect their properties.<sup>62,63</sup> Nanowires,<sup>64</sup> nanotubes,<sup>64,65</sup> nanowhiskers,<sup>66</sup> nanobelts,<sup>67</sup> nanowalls,<sup>68</sup> nanorods,<sup>65,69</sup> hollow spheres,<sup>70</sup> and flowerlike structures<sup>71,72</sup> of copper sulfide were synthesized using various wet chemical methods.<sup>63</sup> Usually, the so-called hydrothermal technique is the most popular synthesis method for copper sulfide synthesis, owing to its simple operation and its use of inexpensive equipment.<sup>73</sup> However, synthesizing a single phase of copper sulfide with controlled morphology has remained a challenge. Many attempts have been made to control phase formation in copper sulfide nanocrystals by controlling the precursor concentration ratios,<sup>74</sup> using various precursor materials,<sup>75</sup> varying the reaction temperatures,<sup>76</sup> and employing different mixtures of stabilizing surfactants.<sup>77</sup> Du et al.<sup>78</sup> presented a simple and efficient solution-phase approach for synthesizing a hexagonal phase of Cu<sub>2</sub>S layered nanocrystals. Recently, Senthilkumar et al.<sup>48</sup> synthesized one-phase hexagonal digenite Cu<sub>9</sub>S<sub>5</sub> nanodisks using toxic solvents.

Additionally, there are few reports of copper sulfide synthesized by other techniques. Liao et al. produced copper sulfide nanorods by microwave-heating, obtaining large quantities of copper sulfide.<sup>73</sup> Reijnen et al.<sup>79,80</sup> deposited thin films of copper sulfide using atomic layer deposition (ALD) and CVD based on Cu(thd)<sub>2</sub> (copper bis-tetramethylheptanedionate) using the toxic compound H<sub>2</sub>S as a precursor. They showed that hydrogen was necessary for copper sulfide growth using CVD while it was not required using ALD. Schneider et al.<sup>81</sup> deposited copper sulfide thin films using ALD of various precursors. They obtained multiphase compound thin films (digenite Cu<sub>9</sub>S<sub>5</sub>, chalcocite Cu<sub>2</sub>S, djurleite Cu<sub>31</sub>S<sub>16</sub>,

and covellite CuS) or single-phase digenite thicker films depending on the number of ALD cycles. Xu et al.<sup>82</sup> reported the use of a catalyst-free and template-free CVD technique for synthesizing 0D and 1D Cu<sub>1.96</sub>S, and layered CuS nanostructures. They showed that the growth temperature is essential for morphology and structure control of different copper sulfides. However, this method included the mixing of hydrogen with sulfur, which resulted in the formation of the toxic H<sub>2</sub>S gas as a byproduct. Recently, Bryks et al.<sup>83</sup> synthesized approximately 4.5 nm thick digenite nanosheets with 2.25 μm width using solventless thermolysis of layered copper alkanethiolate precursors that were synthesized by precipitating Cu(OAc) with HSC<sub>10</sub>H<sub>20</sub>COOH in solution.

Here, we report a facile bottom-up method to synthesize high yields of layered copper sulfide from copper foil and sulfur powder by thermal annealing under an inert gas (Ar). Through extensive characterizations, we show that the material obtained exhibits a unique stoichiometry (digenite, Cu<sub>9</sub>S<sub>5</sub>), is p-type (as expected), exhibits high electrical conductivity, and has a bandgap of 2.5 eV. We also show that we can deposit few-layers and monolayers on a substrate using sonication and dropcasting (top-down). We investigated the electrical conductivity of copper sulfide flakes using peak force tunneling atomic force microscopy (PF-TUNA) and demonstrated that there is a correlation between conductivity and the number of layers. Using a half cell against Li foil, we tested the electrochemical behavior of the bulk Cu<sub>9</sub>S<sub>5</sub>. We found that the capacity obtained in the half cell exceeded the theoretical capacity of sulfur (1645 mA h/g<sub>sulfur</sub>).

The proposed synthesis provides a new p-type layered material, which is a critical building-block for the fabrication of devices such p–n junctions, heterojunctions, and complementary metal-oxide-semiconductor (CMOS) field effect transistors.

## EXPERIMENTAL SECTION

**Synthesis.** We synthesized copper sulfide using a three-zone atmospheric-pressure furnace. The furnace was equipped with a fused-silica (quartz) tube with an internal diameter of 22 mm. Furnace temperatures were monitored using built-in furnace thermocouples. During the growth, the temperatures were set at 450 °C for zones 1 (G<sub>1</sub>) and 2 (G<sub>2</sub>) and 650 °C for zone 3 (G<sub>3</sub>). The flow of argon (99.9999%, from Gas Technologies) was maintained using electronic mass flow controllers (MKS model P4B) with digital mass flow control unit (MKS model 247D).

The synthesis was carried out in three steps. First, we placed a ceramic boat with 1.1 g of sulfur powder (Alfa Aesar, 99.5%, 325 mesh) outside of the furnace, upstream of the gas flow. We also positioned a second boat with a 0.5 cm × 1.5 cm piece of copper foil (Alfa Aesar, 99.9%) downstream, outside the heated zone of the furnace. We purged the quartz tube with argon, while the two boats were kept at room temperature until the furnace reached equilibrium at the desired temperatures in all the three zones, and the reactor was filled with argon. Next, for copper sulfide growth, we pushed the quartz tube inside the furnace to position copper foil in the middle of the growth zone G<sub>3</sub> (650 °C). We then introduced the sulfur boat at the edge of the first zone G<sub>1</sub> inside the furnace (450 °C) using an external magnet. We kept the two boats inside the furnace for 15 min in order to complete the reaction. To end the process, we first pulled out the sulfur boat from G<sub>1</sub>, and then shifted the quartz tube out of the furnace, allowing a fast cool down of the sample to room temperature, under a flow of argon before removing it from the furnace and exposing it to air. We used here the “fast heat” technique which was described in our previous papers.<sup>84</sup> Using this technique, we heated the sample to the desired temperature without exposing it to temperature ramp up or down.

**Copper Sulfide Characterization.** TEM analysis was carried out in LaB6- Jeol-1400 and FEI G12 transmission electron microscopes with an acceleration voltage of 120 kV. Convergent beam electron diffraction (CBED) results were obtained using a 4 nm probe size. Samples were prepared by dispersing a section of the copper sulfide in hexane followed by a gentle sonication for 1 h, and then by placing a single drop of the solution on a 300-mesh Cu lacey carbon grid (from SPI). The Cu<sub>9</sub>S<sub>5</sub> rhombohedral phase and cubic phase were characterized by PDF files 47-1748 and 56-1256, respectively. These files are in agreement with the XRD analysis that indicates the same PDF files.

AFM measurements were carried out using a Bio FastScan scanning probe microscope (Bruker AXS). All images were obtained using tapping mode with a FastScan-A (Bruker) silicon probe (spring constant of 18 N/m). The resonance frequency of the cantilever was approximately 1400 kHz (in air). The measurements were performed under environmental conditions. The images were captured in the retrace direction with a scan rate of 2.0 Hz. The resolution of the images was 512 samples/line. For image processing Nanoscope Analysis software was used. Before analysis of the images, the “flattening” and “plane fit” functions were applied to each image. Samples were prepared in two different ways: first, a solid sample of copper sulfide was attached to a stainless steel (StStl) stab by carbon tape, and part of it was removed using scotch tape. The part of copper sulfide that was left on the stab was examined by AFM. Additionally, we measured copper sulfide flakes on Si/SiO<sub>2</sub> wafer, prepared by a single drop from a copper sulfide dispersion in hexane, after a sonication bath for 1 h.

The theoretical crystal structure was visualized by the VESTA program, using atomic locations from CIF file number 9000079.cif (Crystallography Open Database) and adapting unit cell parameters as recorded in PDF 47-1748.

X-ray powder diffraction measurements were carried out using a Rigaku Smartlab X-ray diffractometer. We crashed the copper sulfide crystals before measuring. Data was collected in the 2 $\theta$  range from 25° to 90°, with a step size of 0.004° and scanning rate of 0.4°/min. The X-ray generator was operated at 40 kV and 30 mA with Cu K $\alpha$  radiation ( $\lambda = 1.542 \text{ \AA}$ ). The two digenite Cu<sub>9</sub>S<sub>5</sub> polymorphs, rhombohedral and cubic phases, were identified by PDF 47-1748 and PDF 56-1256, respectively.

Photoluminescence (PL) was excited using a 1 mW He–Cd laser and was acquired using an optical microscope and a Newport Corp. MS257 spectrometer with long-pass filters to filter out high-order diffractions and a Si CCD detector.

Surface photovoltage spectroscopy (SPV) was measured by monitoring changes in the surface work function. These changes were monitored using the Kelvin probe technique. The latter measures the contact potential difference (CPD), i.e., the difference in work function, between the semiconductor free surface and a vibrating reference probe. A commercial Kelvin probe (Besocke Delta Phi), with a sensitivity of  $\sim 1 \text{ mV}$ , was used in all measurements. The physics of the technique is discussed further in the context of its data. We refer the reader to a thorough review of the method that may be found in ref 85. CPD was recorded as a function of the photon energy, using a xenon light source monochromatized, filtered, and scanned from low to high photon energies while keeping a constant photon flux throughout the measurement.

Thermoelectric probe measurements were carried out using two soldered indium 5 mm spaced contacts, one of which was heated up during the measurement using a soldering iron.<sup>85,86</sup>

**Four-Point Probe Measurements.** A Cu<sub>9</sub>S<sub>5</sub> sample was polished to facilitate an easy calculation of the geometry correction factors. The sample was placed on an insulating substrate (a bare printed circuit board insulator). A 4-point probe was brought into contact with the surface. Current was applied between the two outer contacts, and voltage was measured between the two inner contacts. To calculate the resistivity, we used the following equation,  $\rho = 2\pi sFV/I$ , where  $s$  is the spacing between neighboring probes,  $F$  is a correction factor for sample geometry,  $I$  is the applied current, and  $V$  is the measured voltage. A full description of the correction factor  $F$  may be found in ref 87.

**Hall Effect Measurements.** The Hall effect was measured using the four-point contact method. Due to the brittleness of the samples, soft indium contacts were used. The measurements were carried out at room temperature using homemade permanent magnets.

**PF-TUNA Measurements.** Bulk copper sulfide was mechanically crushed and placed on a conductive substrate of highly oriented pyrolytic graphite (HOPG), attached to a steel stub holder. Local electrical conductivity was measured using a Bruker ICON AFM system equipped with a highly sensitive current detector (PF-TUNA module). A bias voltage of 500 mV was applied to the sample, and the electric current was passed through the AFM tip. The PF-TUNA tip is coated with Pt–Ir conductive coating (SCM-PIT probe, Bruker, spring constant 2.8 N/m, resonant frequency 75 kHz). All PF-TUNA measurements were performed under an optimal loading force of  $\sim 1 \text{ nN}$ . In addition to Cu<sub>9</sub>S<sub>5</sub>, HOPG (lot 492000305, grade ZYH, purchased from Digital Instruments) and MoS<sub>2</sub> (single-crystal large lot 1170529, purchased from SPI SUPPLIES) were exfoliated using an adhesive tape, and placed on a conductive carbon tape attached to a steel stub holder. Local electrical conductivity was measured as before. To compare the different layered materials in terms of resistance/thickness, we used the average current and thickness values of a flake per scan line.

**Electrochemical Characterization.** To evaluate the electrochemical behavior of the Cu<sub>9</sub>S<sub>5</sub> samples, we prepared Cu<sub>9</sub>S<sub>5</sub> composite electrodes. The Cu<sub>9</sub>S<sub>5</sub> was first ball-milled at 600 rpm for 2 min (4 intervals) and then mixed in the following ratios: 80% Cu<sub>9</sub>S<sub>5</sub> as the active material, 10% PVdF as a binder, and 10% carbon black Super-P (TIMCAL). For the slurry preparation, 1-N-methyl-2-pyrrolidone (NMP) was added and mixed together in the Thinky mixer (ARV-310/ARV-310LED) in order to obtain smooth slurries. The electrodes were prepared by coating the slurry onto copper foils using the doctor-blade technique, dried overnight at room temperature, and then heated overnight at 120 °C in a vacuum. Cell assembly was carried out using coin-type cells 2325 (NRC) in an argon-filled dry glovebox (MBraun Inc.). The Li metal foil was used as the counter and reference electrodes in half cell. A porous polyethylene-based membrane (Tonen) was used as the separator. The electrolyte solutions used were 1 M LiPF<sub>6</sub> in fluoroethylene carbonate (FEC) and dimethyl carbonate (DMC) 1:4 mixtures by weight (Merck), as well as dimethoxyethane (DME) and 1,3 dioxolane (DOL) 1:1 1 M LiTFSI with 1.5% LiNO<sub>3</sub>. The cells were stored for 10 h at room temperature after assembling, at an open circuit voltage (OCV), to ensure the complete wetting of the electrodes and the separators with the electrolyte solution. The cells were measured by galvanostatic charge–discharge cycling. Two-electrode Li/Cu<sub>9</sub>S<sub>5</sub> cells were discharged using a BT2000 battery cycler (Arbin Instruments) at 50  $\mu\text{A}$  from OCV to 1.6 and 2 V. The electrochemical measurements were performed at 30 °C.

## RESULTS AND DISCUSSION

We synthesized bulk copper sulfide by thermal annealing using CVD in a three-zone atmospheric-pressure furnace using sulfur powder and copper foil as precursors. The sulfur powder was positioned upstream at the edge of the first zone G<sub>1</sub> (set at 450 °C) while a copper foil was positioned downstream at the center of the third zone G<sub>3</sub> (set at 650 °C), as depicted in Figure 1b. After 15 min of annealing under inert atmosphere (argon), the copper foil transformed into a rough, brittle, and dark blue shiny substance (Figure 1a,c).

SEM images showed a layered morphology (Figure 2). The sample is composed of large sub-millimeter crystals with micron-size texture (Figure 2a). Higher magnifications show a surface texture of oriented triangles demonstrating the single-crystalline nature of each sub-millimeter crystallite (Figure 2b,c).

AFM image (Figure 3) confirmed the layered structure of the Cu<sub>9</sub>S<sub>5</sub>. While each terrace is tens of nm thick, the terraces

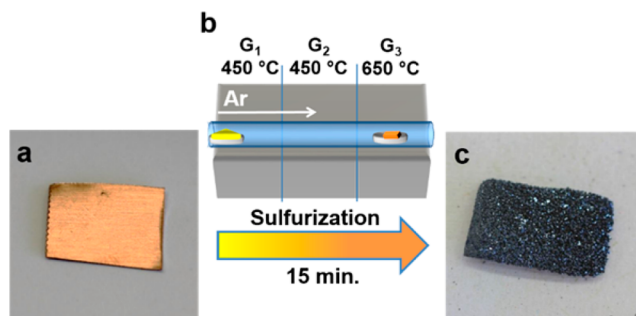


**Figure 1.** (a) Pristine copper foil before treatment. (b) Scheme of the CVD system and positions of the sulfur powder (left, G<sub>1</sub>) and copper foil (right, G<sub>3</sub>) inside the furnace. (c) Copper foil after sulfurization, transformed into a shiny dark blue copper sulfide.

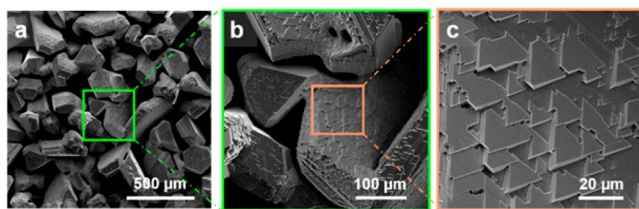


**Figure 2.** SEM images of layered Cu<sub>9</sub>S<sub>5</sub>: (a) Low magnification presents sub-millimeter sized crystallites. (b) Further magnification resolves layered texture of thin triangles. (c) All triangles are in perfect stoichiometric relations suggesting that the millimeter-sized grains are single crystals.

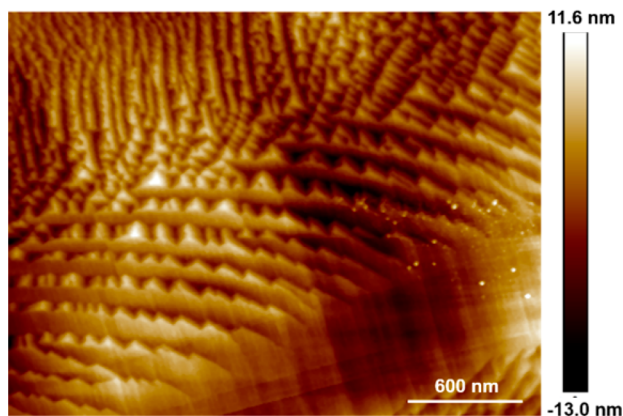


**Figure 3.** AFM image of layered Cu<sub>9</sub>S<sub>5</sub> confirmed the layered structure observed with SEM.

observed in the as-grown material were still too thick to represent monolayers.

After sonication of a dispersion of the crushed material in hexane and dropcasting a drop of the solution on a Si/SiO<sub>2</sub> wafer, we observed flakes of different thicknesses: monolayers, bilayers, and few-layers. The thickness of the deposited monolayer flakes was measured using AFM and is shown in Figure 4a. It suggests a monolayer thickness of about 1.2 ± 0.3 nm, which is in agreement with a rhombohedral structure based on a theoretical model<sup>88</sup> of the Cu<sub>9</sub>S<sub>5</sub> (the model is shown in Figure 4b). Figure 4c, a lower-magnification AFM image (20 × 20 μm<sup>2</sup>), shows a vast coverage of bilayers and monolayers. According to an adhesion map (Figure S1, Supporting Information), there was only a single material on the SiO<sub>2</sub> substrate, without any significant contamination. SEM images

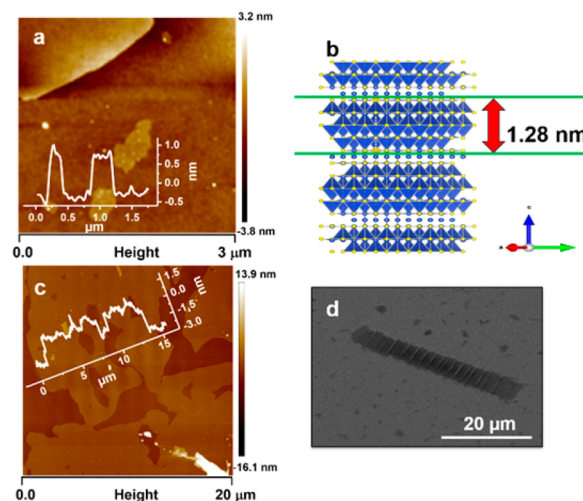


**Figure 4.** (a) AFM measurements of a dispersed Cu<sub>9</sub>S<sub>5</sub> demonstrated minimal thickness of 1.2 ± 0.3 nm; the measurements were carried out on more than 10 flakes. (b) Theoretical structure model. (c) Wide-scale AFM image (20 × 20 μm<sup>2</sup>) of a Cu<sub>9</sub>S<sub>5</sub> dispersion. (d) SEM image of an isolated Cu<sub>9</sub>S<sub>5</sub> flake.

of the dropcast Cu<sub>9</sub>S<sub>5</sub> show few-layered large flakes with sizes exceeding 40 × 5 μm<sup>2</sup> (Figure 4d).

We performed phase analysis of the crushed copper sulfide crystals using XRD. The XRD spectrum (Figure 5a) contains a

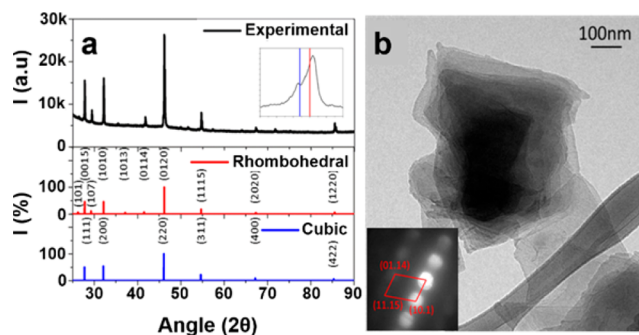


**Figure 5.** (a) XRD pattern of crushed copper sulfide crystals. Peak positions and intensities from the literature are indicated in the figure for two digenite Cu<sub>9</sub>S<sub>5</sub> polymorphs: a rhombohedral phase (red) and a cubic phase (blue). The inset shows the split of the peak located at 2θ = 32.1 into the two polymorphs. (b) TEM image and CBED analysis confirm the layered copper sulfide as being a rhombohedral Cu<sub>9</sub>S<sub>5</sub> phase.

consistent split of many peaks and indicates the presence of two polymorphs of digenite, Cu<sub>9</sub>S<sub>5</sub>: the first, a rhombohedral phase, space group  $R\bar{3}m$ , with  $a = 3.93 \text{ \AA}$  and  $c = 48.14 \text{ \AA}$ ; and the second, a cubic phase, space group  $Fm\bar{3}m$ , with  $a = 5.571 \text{ \AA}$ . We hypothesize that, by using the “fast heat” method (that we extensively applied to carbon nanotube synthesis using CVD),<sup>84</sup> which minimizes the thermal dose through rapid temperature transitions, specific kinetic processes were favored, leading to a unique stoichiometry and limiting the formation of mixed phases in the obtained products.

From correlation between TEM images and converged microbeam electron diffraction (CBED) analysis, it is apparent that each phase holds a different layout (Figure 5b). The Cu<sub>9</sub>S<sub>5</sub> rhombohedral phase is clearly layered and stacking 2D layers, one on top of the other to form pyramids (or bipyramids) that

are eventually arranged in the observed triangles. On the other hand, the cubic phase appears polycrystalline and less defined in shape (see Figure S2 in Supporting Information).

To gain insight into the semiconductor properties of this material, we carried out photoluminescence (PL) spectroscopy measurements on the as-grown  $\text{Cu}_9\text{S}_5$  sample. Figure 6a

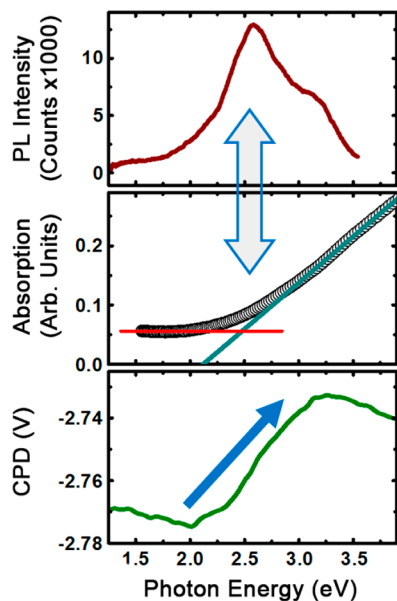


**Figure 6.** (a) Photoluminescence spectrum of the synthesized bulk  $\text{Cu}_9\text{S}_5$ . (b) Absorption spectrum of a  $\text{Cu}_9\text{S}_5$  dispersion showing the absorption edge  $\sim 2.5$  eV. (c) Surface photovoltage spectrum obtained from the same  $\text{Cu}_9\text{S}_5$  sample as the PL showing a rise over the same energy range indicating a p-type conductivity.

presents two peaks: the main peak is about 1 eV wide and centered at about 2.6 eV, and a second peak, of relatively small intensity, is seen to ride the shoulder of the main peak and is centered at about 3.25 eV. We also performed absorption spectroscopy using a quartz cuvette containing the dispersion that was previously used for the TEM analysis and observed a rise in absorption around 2.5 eV (Figure 6b). If this rise represents the absorption edge of the material, then it correlates with the main PL peak, suggesting that this is the bandgap of the material. Surface photovoltage spectroscopy carried out over the same spectral range as the two other spectroscopy measurements shows a rise in the contact potential difference (CPD) over the same energy range as the PL spectrum (Figure 6c). The surface photovoltage is defined as the difference between the CPD in the dark and the CPD under illumination. Under illumination, p-type semiconductor energy bands are bent downward toward the surface, whereas those in n-type semiconductors are bent upward. Illumination with photons of energy greater than the bandgap typically tends to decrease the surface band-bending. Due to the different signs of the equilibrium surface potential, a CPD rise at the bandgap energy of the material means that the material is of p-type conductivity.<sup>85</sup> Thus, photoluminescence, absorption spectroscopy, and surface photovoltage spectroscopy are all consistent with a bandgap of about 2.5 eV.

Since cation vacancies are known to plague most of the Cu(I) compounds, we expect copper sulfides to show p-type conductivity.<sup>42,46</sup> To further verify the conductivity type, we used the thermoelectric probe method. We characterized the

Seebeck current between the contacts using the electrical circuit shown in the inset of Figure 7. At first, the grounded contact

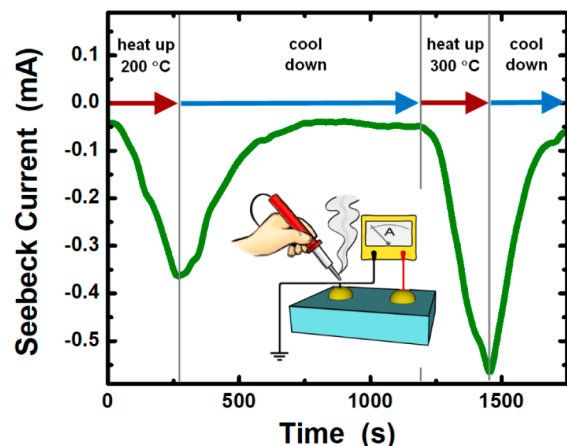


**Figure 7.** Thermoelectric probe carried out on the synthesized bulk  $\text{Cu}_9\text{S}_5$  showing the Seebeck current behavior in time at two consecutive experiments wherein one contact was heated up and let to cool down. The polarity of the current change indicates conduction by holes, i.e., p-type conductivity.

was heated up to about 200 °C. As a result, the current was observed to grow negative. Then, the heat source was turned off, and the sample was let to cool down, at which stage the current became less negative. The process was then repeated a second time at a higher temperature of 300 °C, and the same current behavior was observed only to a greater extent. The meaning of the negative current is that the current flows from the hot contact to the cold contact suggesting that the conductivity is indeed carried out by holes.

As is commonly the case with copper-containing materials, our  $\text{Cu}_9\text{S}_5$  appears to be a good conductor. Copper-containing compounds have always been a subject for superconductivity testing. Specifically, there have been reports of superconductive behavior in very close compounds, e.g.,  $\text{CuSe}$ .<sup>89</sup> Hall effect measurements performed on the bulk  $\text{Cu}_9\text{S}_5$  showed mobilities of  $\sim 1$   $\text{cm}^2/(\text{V s})$ .

The conductivity measured using a 4-point probe on bulk samples was very high, above 45  $(\Omega \text{ cm})^{-1}$ . This corresponds to high hole concentrations on the order of  $10^{20} \text{ cm}^{-3}$ . While these numbers are preliminary and require more statistics, they do not seem to be in line with the surface photovoltage results which appear to suggest a more moderately doped semiconductor. However, this measured high conductivity is consistent with a recent theoretical study that suggests an inherently high hole concentration in this p-type material.<sup>90</sup> This very high level of doping is also in line with the low mobility observed, which may be due to impurity scattering,<sup>91</sup> possibly compounded by grain boundary scattering that is also known to limit mobility.<sup>92</sup>

2D materials are known to have nonisotropic conductivity, i.e., show better conductivity within a layer than between the layers.<sup>93</sup> To map the conductivity of different areas in the sample related to the topography of the sample, we used PF-TUNA, which can detect the electrical conductivity only along the z-axis of the flake. We investigated the electrical properties of our copper sulfide (mechanically exfoliated) on a highly oriented pyrolytic graphite (HOPG) substrate by simultaneous measure of the thickness of the flakes and of the current passed

through it. Figure 8 shows an AFM topography image combined with a TUNA current image of the flakes. Since

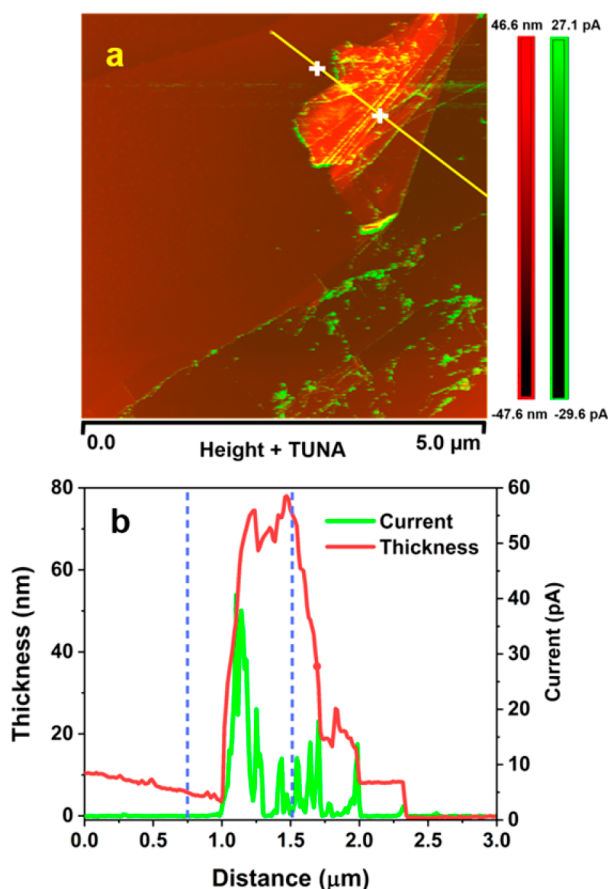


**Figure 8.** (a) PF-TUNA topography and current combined image of  $\text{Cu}_9\text{S}_5$  flakes and their cross sections for a DC sample bias of 500 mV. (b) A current profile along the yellow line shows a staircase structure on its right shoulder, i.e., an increase of the current with the sample thickness. The dashed blue lines present the position of the white crosses on the image.

we used crushed bulk  $\text{Cu}_9\text{S}_5$  for PF-TUNA measurements (thick flakes), both the rhombohedral and the cubic phase may have been present, thus making it difficult to correlate between the conductivity and the crystal structure of the material. However, given that TEM imaging (Figure 5b) showed that only the rhombohedral phase was layered, we can speculate that the thick flakes we measured with PF-TUNA were made of the rhombohedral phase.

The observed results indicated that  $\text{Cu}_9\text{S}_5$  is electrically conductive. When applying a dc sample bias of 500 mV, a current was detected on the defects and the edges of the flake. Previous work<sup>94,95</sup> on the conductivity of  $\text{MoS}_2$  flakes suggested that flakes with defects (vacancies resulted from losing sulfur atoms) on the surface edges exhibit greater conductivity along the flake edges compared to the center of the flake. The interaction of the sample surface with the AFM tip may be different at the center of the flake compared to its edges. When the tip scans the center of the flake, only its sharp end interacts with the surface; thus, the contact between the tip and the flake is limited to a very small area. The consequence is that only very small currents can be detected.<sup>96</sup> However, when the tip scans the edges of the flake, the interaction occurs over a much

larger surface. This increase in contact area enables measuring higher currents. We assume that a combination of these factors may lead to the observed higher currents at the edges of the flake and on larger defects. In addition, Figure 8 shows an increase in conductivity as the number of layers increases, similar to the findings reported by Song et al.<sup>96</sup> on the conductivity of  $\text{MoS}_2$  flakes.

We also used PF-TUNA to compare the resistance of our mechanically exfoliated  $\text{Cu}_9\text{S}_5$  to highly oriented pyrolytic graphite (HOPG), and to  $\text{MoS}_2$  (both with many-layers). Although this is a 2-point electrical measurement that does not allow separation of the contact resistance from the total resistance measured, the ratio of the resistances over their measured thicknesses provides a good comparison between these materials. We then calculated the “resistivity ratio” among the materials in relation to HOPG resistivity using eq 1:

$$\frac{\rho_{\text{mat}}}{\rho_{\text{HOPG}}} = \frac{I_{\text{HOPG}} \times t_{\text{HOPG}}}{I_{\text{mat}} \times t_{\text{mat}}} \quad (1)$$

where  $I_{\text{mat}}$  and  $t_{\text{mat}}$  are current and thickness of the specific material, and  $I_{\text{HOPG}}$  and  $t_{\text{HOPG}}$  are current and thickness of HOPG measured by PF-TUNA, respectively. We assume that the area of the contact and voltage are the same in all measurements.

We observed that the resistivity ratio (compared to HOPG) of  $\text{Cu}_9\text{S}_5$  (2.5 eV bandgap for bulk) was 187, while that of  $\text{MoS}_2$  (1.2 eV bandgap for bulk<sup>11</sup>) was 8463; this makes  $\text{Cu}_9\text{S}_5$  45 times more conductive than  $\text{MoS}_2$ . Please note that we refer here to bulk measurements since the average measured thickness was over 16 nm. The obtained resistivity ratio between  $\text{MoS}_2$  and HOPG is similar to recent reports.<sup>97,98</sup>

These results are also consistent with our 4-point probe measurements, and in line with a theoretical study indicating that high p-doping levels are to be expected in  $\text{Cu}_9\text{S}_5$ .<sup>90</sup>

Sulfur-containing materials are considered as potential next-generation electrodes for lithium-ion batteries.<sup>26</sup> This property, together with the discovery of the layered feature of our  $\text{Cu}_9\text{S}_5$ , led us to investigate its electrochemical behavior. A  $\text{Cu}_9\text{S}_5$  composite electrode was set in a half cell against Li foil and reduced galvanostatically to a cutoff voltage of 1.5 V versus Li. The material exhibited a very high capacity of  $\sim 500$  mA h/g<sub>digenite</sub> and nearly 2000 mA h/g<sub>sulfur</sub>. The high value of capacity per sulfur strongly suggests an enhancement in the electrochemical activity, since the material exceeds the theoretical capacity of sulfur (1645 mA h/g<sub>sulfur</sub>). A mechanistic approach to the enhanced electrochemical activity is currently under investigation and is beyond the scope of the current manuscript. In general, two electrochemically induced phase changes were observed upon lithiation at 2.1 and 1.7 V. The  $\text{Cu}_9\text{S}_5$  electrode and consequent phase change products were characterized by XRD (Figure S3). In the first plateau, we found that the electrode phase changed from digenite ( $\text{Cu}_9\text{S}_5$ ) to chalcocite ( $\text{Cu}_2\text{S}$ ). In the second plateau, the obtained  $\text{Cu}_2\text{S}$  reduced completely to Cu while  $\text{Li}_2\text{S}$  compound was formed. Surprisingly, we were able to demonstrate a galvanostatic charge/discharge profile, not only in DOL:DME-based electrolyte solution, but also in an alkyl carbonate electrolyte, which is generally known to produce an irreversible electrochemical reaction for sulfur redox. The charge/discharge profiles are presented in Figure 9.

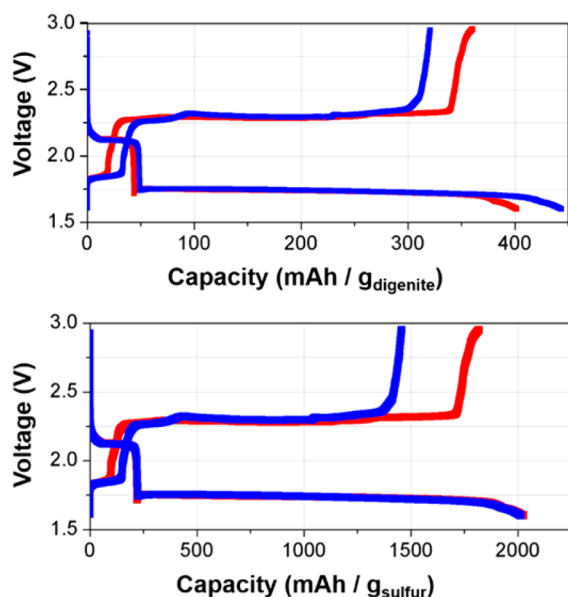


**Figure 9.** Voltage profiles obtained from  $\text{Cu}_9\text{S}_5$  electrodes in half cell configuration at the 1st cycle normalized to sulfur mass (down) and electrode mass (up) with DME:DOL 1:1 1 M LiTFSI 1.5% wt %  $\text{LiNO}_3$  (red) and FEC:DMC 1:4 1 M  $\text{LiPF}_6$  (blue) as electrolyte solution.

## CONCLUSION

We report a simple CVD method to grow high yields of bulk layered copper sulfide. The material exhibits a single stoichiometry ( $\text{Cu}_9\text{S}_5$ ) and two crystal structures: a cubic phase and a rhombohedral phase. The rhombohedral phase was found to possess a layered structure, with layers tens of nm thick, which are themselves composed of monolayers that we were able to separate and to deposit on a substrate after liquid exfoliation and dropcasting. Using multiple characterizations, we demonstrated that the material is p-type with a bandgap of about 2.5 eV. We showed that  $\text{Cu}_9\text{S}_5$  is electrically very conductive (above  $45 (\Omega \text{ cm})^{-1}$ ) and that the electrical conductivity increased with the number of layers. Initial electrochemical measurements demonstrated that  $\text{Cu}_9\text{S}_5$  exhibited a high capacity of  $\sim 500 \text{ mA h/g}_{\text{digenite}}$  and nearly  $2000 \text{ mA h/g}_{\text{sulfur}}$  exceeding the theoretical capacity of sulfur ( $1645 \text{ mA h/g}_{\text{sulfur}}$ ). We are currently investigating this enhancement in the electrochemical activity. This method introduces a new p-type layered material that has the potential to be used for Li-ion batteries and supercapacitors. Additionally, after exfoliation and dropcasting, it has the potential to be combined with the many available n-type monolayer materials (e.g., TMDs) to fabricate original p–n junctions and CMOS transistors.

## ASSOCIATED CONTENT

### Supporting Information

The Supporting Information is available free of charge on the ACS Publications website at DOI: [10.1021/acs.chemmater.8b00191](https://doi.org/10.1021/acs.chemmater.8b00191).

TEM images of the cubic and the rhombohedral phases, AFM image of the adhesion forces in the monolayer sample, and XRD characterization of the different copper sulfide phases in the Li-ion half cell (PDF)

## AUTHOR INFORMATION

### Corresponding Authors

\*E-mail: [shalish@bgu.ac.il](mailto:shalish@bgu.ac.il)

\*E-mail: [gdnessim@biu.ac.il](mailto:gdnessim@biu.ac.il)

### ORCID

Gilbert Daniel Nessim: 0000-0003-0738-5436

### Author Contributions

<sup>||</sup>A.I. and E.T. contributed equally as first authors. I.S. and G.D.N. contributed equally as corresponding authors. The manuscript was written through the contributions of all authors. All authors have given approval to the final version of the manuscript.

### Notes

The authors declare no competing financial interest.

## ACKNOWLEDGMENTS

G.D.N. and M.N. would like to thank the Israel Science Foundation and Israel Prime Minister's Office fuel alternatives initiative for partial funding of this study under the Israel Research center for Electrochemical Propulsion (INREP) (Grant: ISF 2797/11). O.G. and collaborators thank the International Atomic Energy Agency (IAEA) for partial support. E.S.A. would like to thank the Israeli ministry of science, technology, and space for their financial support.

## REFERENCES

- (1) Novoselov, K. S.; Geim, A. K.; Morozov, S. V.; Jiang, D.; Zhang, Y.; Dubonos, S. V.; Grigorieva, I. V.; Firsov, A. A. Electric Field Effect in Atomically Thin Carbon Films. *Science* **2004**, *306*, 666–669.
- (2) Novoselov, K. Graphene: The Magic of Flat Carbon. *Electrochem. Soc. Interface* **2011**, *20*, 45–46.
- (3) Novoselov, K. S.; Jiang, D.; Schedin, F.; Booth, T. J.; Khotkevich, V. V.; Morozov, S. V.; Geim, A. K. Two-Dimensional Atomic Crystals. *Proc. Natl. Acad. Sci. U. S. A.* **2005**, *102*, 10451–10453.
- (4) Avouris, P. Graphene: Electronic and Photonic Properties and Devices. *Nano Lett.* **2010**, *10*, 4285–4294.
- (5) Kim, K. S.; Walter, A. L.; Moreschini, L.; Seyller, T.; Horn, K.; Rotenberg, E.; Bostwick, A. Coexisting Massive and Massless Dirac Fermions in Symmetry-Broken BiLayer Graphene. *Nat. Mater.* **2013**, *12*, 887–892.
- (6) Xia, F. N.; Farmer, D. B.; Lin, Y. M.; Avouris, P. Graphene Field-Effect Transistors with High On/Off Current Ratio and Large Transport Band Gap at Room Temperature. *Nano Lett.* **2010**, *10*, 715–718.
- (7) Frindt, R. F. Single Crystals of  $\text{MoS}_2$  Several Molecular Layers Thick. *J. Appl. Phys.* **1966**, *37*, 1928–1929.
- (8) Joensen, P.; Frindt, R. F.; Morrison, S. R. Single-Layer  $\text{MoS}_2$ . *Mater. Res. Bull.* **1986**, *21*, 457–461.
- (9) Butler, S. Z.; Hollen, S. M.; Cao, L. Y.; Cui, Y.; Gupta, J. A.; Gutierrez, H. R.; Heinz, T. F.; Hong, S. S.; Huang, J. X.; Ismach, A. F.; Johnston-Halperin, E.; Kuno, M.; Plashnitsa, V. V.; Robinson, R. D.; Ruoff, R. S.; Salahuddin, S.; Shan, J.; Shi, L.; Spencer, M. G.; Terrones, M.; Windl, W.; Goldberger, J. E. Progress, Challenges, and Opportunities in Two-Dimensional Materials Beyond Graphene. *ACS Nano* **2013**, *7*, 2898–2926.
- (10) Bhimanapati, G. R.; Lin, Z.; Meunier, V.; Jung, Y.; Cha, J.; Das, S.; Xiao, D.; Son, Y.; Strano, M. S.; Cooper, V. R.; Liang, L. B.; Louie, S. G.; Ringe, E.; Zhou, W.; Kim, S. S.; Naik, R. R.; Sumpter, B. G.; Terrones, H.; Xia, F. N.; Wang, Y. L.; Zhu, J.; Akinwande, D.; Alem, N.; Schuller, J. A.; Schaak, R. E.; Terrones, M.; Robinson, J. A. Recent Advances in Two-Dimensional Materials beyond Graphene. *ACS Nano* **2015**, *9*, 11509–11539.
- (11) Koski, K. J.; Cui, Y. The New Skinny in Two-Dimensional Nanomaterials. *ACS Nano* **2013**, *7*, 3739–3743.

- (12) Shi, Y. M.; Li, H. N.; Li, L. Recent Advances in Controlled Synthesis of Two-Dimensional Transition Metal Dichalcogenides via Vapour Deposition Techniques. *Chem. Soc. Rev.* **2015**, *44*, 2744–2756.
- (13) Xie, L. M. Two-Dimensional Transition Metal Dichalcogenide Alloys: Preparation, Characterization and Applications. *Nanoscale* **2015**, *7*, 18392–18401.
- (14) Mas-Balleste, R.; Gomez-Navarro, C.; Gomez-Herrero, J.; Zamora, F. 2D Materials: to Graphene and Beyond. *Nanoscale* **2011**, *3*, 20–30.
- (15) Zhang, Y.; Chang, T. R.; Zhou, B.; Cui, Y. T.; Yan, H.; Liu, Z. K.; Schmitt, F.; Lee, J.; Moore, R.; Chen, Y. L.; Lin, H.; Jeng, H. T.; Mo, S. K.; Hussain, Z.; Bansil, A.; Shen, Z. X. Direct Observation of the Transition From Indirect to Direct Bandgap in Atomically Thin Epitaxial MoSe<sub>2</sub>. *Nat. Nanotechnol.* **2014**, *9*, 111–115.
- (16) Radisavljevic, B.; Radenovic, A.; Brivio, J.; Giacometti, V.; Kis, A. Single-Layer MoS<sub>2</sub> Transistors. *Nat. Nanotechnol.* **2011**, *6*, 147–150.
- (17) Kaasbjerg, K.; Thygesen, K. S.; Jacobsen, K. W. Phonon-Limited Mobility in n-Type Single-Layer MoS<sub>2</sub> From First Principles. *Phys. Rev. B: Condens. Matter Mater. Phys.* **2012**, *85*, 115317–115316.
- (18) Oriakhi, C. O.; Lerner, M. M. *Layered Metal Chalcogenides*; Marcel Dekker: New York, 2004.
- (19) Mak, K. F.; Lee, C.; Hone, J.; Shan, J.; Heinz, T. F. Atomically Thin MoS<sub>2</sub>: A New Direct-Gap Semiconductor. *Phys. Rev. Lett.* **2010**, *105*, 136805-1–136805-4.
- (20) Splendiani, A.; Sun, L.; Zhang, Y. B.; Li, T. S.; Kim, J.; Chim, C. Y.; Galli, G.; Wang, F. Emerging Photoluminescence in Monolayer MoS<sub>2</sub>. *Nano Lett.* **2010**, *10*, 1271–1275.
- (21) Wang, H.; Yu, L. L.; Lee, Y. H.; Shi, Y. M.; Hsu, A.; Chin, M. L.; Li, L. J.; Dubey, M.; Kong, J.; Palacios, T. Integrated Circuits Based on Bilayer MoS<sub>2</sub> Transistors. *Nano Lett.* **2012**, *12*, 4674–4680.
- (22) Pu, J.; Yomogida, Y.; Liu, K.-K.; Li, L.-J.; Iwasa, Y.; Takenobu, T. Highly Flexible MoS<sub>2</sub> Thin-Film Transistors with Ion Gel Dielectrics. *Nano Lett.* **2012**, *12*, 4013–4017.
- (23) Bernardi, M.; Palumbo, M.; Grossman, J. C. Extraordinary Sunlight Absorption and One Nanometer Thick Photovoltaics Using Two-Dimensional Monolayer Materials. *Nano Lett.* **2013**, *13*, 3664–3670.
- (24) Hsu, W. T.; Zhao, Z. A.; Li, L. J.; Chen, C. H.; Chiu, M. H.; Chang, P. S.; Chou, Y. C.; Chang, W. H. Second Harmonic Generation from Artificially Stacked Transition Metal Dichalcogenide Twisted Bilayers. *ACS Nano* **2014**, *8*, 2951–2958.
- (25) Lopez-Sanchez, O.; Lembke, D.; Kayci, M.; Radenovic, A.; Kis, A. Ultrasensitive Photodetectors Based on Monolayer MoS<sub>2</sub>. *Nat. Nanotechnol.* **2013**, *8*, 497–501.
- (26) Yoon, Y.; Ganapathi, K.; Salahuddin, S. How Good Can Monolayer MoS<sub>2</sub> Transistors Be? *Nano Lett.* **2011**, *11*, 3768–3773.
- (27) Yu, W. J.; Li, Z.; Zhou, H. L.; Chen, Y.; Wang, Y.; Huang, Y.; Duan, X. F. Vertically Stacked Multi-Heterostructures of Layered Materials for Logic Transistors and Complementary Inverters. *Nat. Mater.* **2013**, *12*, 246–252.
- (28) Chang, K.; Chen, W. X. In Situ Synthesis of MoS<sub>2</sub>/Graphene Nanosheet Composites With Extraordinarily High Electrochemical Performance for Lithium Ion Batteries. *Chem. Commun.* **2011**, *47*, 4252–4254.
- (29) Lee, C.; Li, Q. Y.; Kalb, W.; Liu, X. Z.; Berger, H.; Carpick, R. W.; Hone, J. Frictional Characteristics of Atomically Thin Sheets. *Science* **2010**, *328*, 76–80.
- (30) Laursen, A. B.; Kegnaes, S.; Dahl, S.; Chorkendorff, I. Molybdenum Sulfides-Efficient and Viable Materials for Electro- and Photoelectrocatalytic Hydrogen Evolution. *Energy Environ. Sci.* **2012**, *5*, 5577–5591.
- (31) Zhan, Y. J.; Liu, Z.; Najmaei, S.; Ajayan, P. M.; Lou, J. Large-Area Vapor-Phase Growth and Characterization of MoS<sub>2</sub> Atomic Layers on a SiO<sub>2</sub> Substrate. *Small* **2012**, *8*, 966–971.
- (32) Yuan, J. T.; Wu, J. J.; Hardy, W. J.; Loya, P.; Lou, M.; Yang, Y. C.; Najmaei, S.; Jiang, M. L.; Qin, F.; Keyshar, K.; Ji, H.; Gao, W. L.; Bao, J. M.; Kono, J.; Natelson, D.; Ajayan, P. M.; Lou, J. Facile Synthesis of Single Crystal Vanadium Disulfide Nanosheets by Chemical Vapor Deposition for Efficient Hydrogen Evolution Reaction. *Adv. Mater.* **2015**, *27*, 5605–5609.
- (33) Lee, Y. H.; Zhang, X. Q.; Zhang, W. J.; Chang, M. T.; Lin, C. T.; Chang, K. D.; Yu, Y. C.; Wang, J. T. W.; Chang, C. S.; Li, L. J.; Lin, T. W. Synthesis of Large-Area MoS<sub>2</sub> Atomic Layers with Chemical Vapor Deposition. *Adv. Mater.* **2012**, *24*, 2320–2325.
- (34) Bilgin, I.; Liu, F. Z.; Vargas, A.; Winchester, A.; Man, M. K. L.; Upmanyu, M.; Dani, K. M.; Gupta, G.; Talapatra, S.; Mohite, A. D.; Kar, S. Chemical Vapor Deposition Synthesized Atomically Thin Molybdenum Disulfide with Optoelectronic-Grade Crystalline Quality. *ACS Nano* **2015**, *9*, 8822–8832.
- (35) Huang, Y.; Sutter, E.; Shi, N. N.; Zheng, J. B.; Yang, T. Z.; Englund, D.; Gao, H. J.; Sutter, P. Reliable Exfoliation of Large-Area High-Quality Flakes of Graphene and Other Two-Dimensional Materials. *ACS Nano* **2015**, *9*, 10612–10620.
- (36) Bojdys, M. J.; Severin, N.; Rabe, J. P.; Cooper, A. I.; Thomas, A.; Antonietti, M. Exfoliation of Crystalline 2D Carbon Nitride: Thin Sheets, Scrolls and Bundles via Mechanical and Chemical Routes. *Macromol. Rapid Commun.* **2013**, *34*, 850–854.
- (37) Huo, C. X.; Yan, Z.; Song, X. F.; Zeng, H. B. 2D Materials via Liquid Exfoliation: a Review on Fabrication and Applications. *Sci. Bull.* **2015**, *60*, 1994–2008.
- (38) Wang, N.; Xu, Q.; Xu, S. S.; Qi, Y. H.; Chen, M.; Li, H. X.; Han, B. X. High-Efficiency Exfoliation of Layered Materials into 2D Nanosheets in Switchable CO<sub>2</sub>/Surfactant/H<sub>2</sub>O System. *Sci. Rep.* **2015**, *5*, 16764–16769.
- (39) Pralong, V. Lithium Intercalation into Transition Metal Oxides: A Route to Generate New Ordered Rock Salt Type Structure. *Prog. Solid State Chem.* **2009**, *37*, 262–277.
- (40) Chang, Y. H.; Zhang, W.; Zhu, Y.; Han, Y.; Pu, J.; Chang, J. K.; Hsu, W. T.; Huang, J. K.; Hsu, C. L.; Chiu, M. H.; Takenobu, T.; Li, H.; Wu, C. I.; Chang, W. H.; Wee, A. T. S.; Li, L. J. Monolayer MoSe<sub>2</sub> Grown by Chemical Vapor Deposition for Fast Photodetection. *ACS Nano* **2014**, *8*, 8582–8590.
- (41) Wang, X. L.; Gong, Y. J.; Shi, G.; Chow, W. L.; Keyshar, K.; Ye, G. L.; Vajtai, R.; Lou, J.; Liu, Z.; Ringe, E.; Tay, B. K.; Ajayan, P. M. Chemical Vapor Deposition Growth of Crystalline Mono layer MoS<sub>2</sub>. *ACS Nano* **2014**, *8*, 5125–5131.
- (42) Raebiger, H.; Lany, S.; Zunger, A. Origins of the p-Type Nature and Cation Deficiency in Cu<sub>2</sub>O and Related Materials. *Phys. Rev. B: Condens. Matter Mater. Phys.* **2007**, *76*, 0452091-1–0452091-5.
- (43) Castellanos-Gomez, A. Black Phosphorus: Narrow Gap, Wide Applications. *J. Phys. Chem. Lett.* **2015**, *6*, 4280–4291.
- (44) Chuang, S.; Battaglia, C.; Azcatl, A.; McDonnell, S.; Kang, J. S.; Yin, X. T.; Tosun, M.; Kapadia, R.; Fang, H.; Wallace, R. M.; Javey, A. MoS<sub>2</sub> p-Type Transistors and Diodes Enabled by High Work Function MoO<sub>x</sub> Contacts. *Nano Lett.* **2014**, *14*, 1337–1342.
- (45) Nipane, A.; Karmakar, D.; Kaushik, N.; Karande, S.; Lodha, S. Few-Layer MoS<sub>2</sub> p-Type Devices Enabled by Selective Doping Using Low Energy Phosphorus Implantation. *ACS Nano* **2016**, *10*, 2128–2137.
- (46) Comin, A.; Manna, L. New Materials for Tunable Plasmonic Colloidal Nanocrystals. *Chem. Soc. Rev.* **2014**, *43*, 3957–3975.
- (47) van der Stam, W.; Berends, A. C.; Donega, C. D. Prospects of Colloidal Copper Chalcogenide Nanocrystals. *ChemPhysChem* **2016**, *17*, 559–581.
- (48) Senthilkumar, M.; Babu, S. M. Synthesis and Characterization of Hexagonal Faceted Copper Sulfide (Cu<sub>1.8</sub>S) Nanodisks. *Mater. Sci. Semicond. Process.* **2015**, *40*, 203–208.
- (49) He, Y.; Day, T.; Zhang, T. S.; Liu, H. L.; Shi, X.; Chen, L. D.; Snyder, G. High Thermoelectric Performance in Non-Toxic Earth-Abundant Copper Sulfide. *Adv. Mater.* **2014**, *26*, 3974–3978.
- (50) Liang, W.; Whangbo, M. H. Conductivity Anisotropy and Structural Phase-Transition in Covellite CuS. *Solid State Commun.* **1993**, *85*, 405–408.
- (51) Paul, P. P.; Rauchfuss, T. B.; Wilson, S. R. General-Synthesis of Metalloid Polysulfide Complexes From the Elements - Structures of Sb<sub>2</sub>S<sub>15</sub><sup>(2-)</sup> and InS<sub>8</sub>(N-meim). *J. Am. Chem. Soc.* **1993**, *115*, 3316–3317.

- (52) Chung, J. S.; Sohn, H. J. Electrochemical Behaviors of CuS as a Cathode Material for Lithium Secondary Batteries. *J. Power Sources* **2002**, *108*, 226–231.
- (53) Raj, C. J.; Kim, B. C.; Cho, W. J.; Lee, W. G.; Seo, Y.; Yu, K. H. Electrochemical Capacitor Behavior of Copper Sulfide (CuS) Nanoplatelets. *J. Alloys Compd.* **2014**, *586*, 191–196.
- (54) Han, Y.; Wang, Y. P.; Gao, W. H.; Wang, Y. J.; Jiao, L. F.; Yuan, H. T.; Liu, S. X. Synthesis of Novel CuS with Hierarchical Structures and its Application in Lithium-Ion Batteries. *Powder Technol.* **2011**, *212*, 64–68.
- (55) Sankapal, B. R.; Mane, R. S.; Lokhande, C. D. Successive Ionic Layer Adsorption and Reaction (SILAR) Method for the Deposition of Large Area (Similar to 10 cm<sup>2</sup>) Tin Disulfide (SnS<sub>2</sub>) Thin Films. *Mater. Res. Bull.* **2000**, *35*, 2027–2035.
- (56) Ornelas-Acosta, R. E.; Shaji, S.; Avellaneda, D.; Castillo, G. A.; Das Roy, T. K.; Krishnan, B. Thin Films of Copper Antimony Sulfide: A Photovoltaic Absorber Material. *Mater. Res. Bull.* **2015**, *61*, 215–225.
- (57) Myung, Y.; Jang, D. M.; Cho, Y. J.; Kim, H. S.; Park, J.; Kim, J. U.; Choi, Y.; Lee, C. J. Nonenzymatic Amperometric Glucose Sensing of Platinum, Copper Sulfide, and Tin Oxide Nanoparticle-Carbon Nanotube Hybrid Nanostructures. *J. Phys. Chem. C* **2009**, *113*, 1251–1259.
- (58) Goel, S.; Chen, F.; Cai, W. B. Synthesis and Biomedical Applications of Copper Sulfide Nanoparticles: From Sensors to Theranostics. *Small* **2014**, *10*, 631–645.
- (59) Vinokurov, K.; Elimelech, O.; Millo, O.; Banin, U. Copper Sulfide Nanocrystal Level Structure and Electrochemical Functionality towards Sensing Applications. *ChemPhysChem* **2016**, *17*, 675–680.
- (60) Zhang, Y.; Qiao, Z. P.; Chen, X. M. Microwave-Assisted Elemental Direct Reaction Route to Nanocrystalline Copper Chalcogenides CuSe and Cu<sub>2</sub>Te. *J. Mater. Chem.* **2002**, *12*, 2747–2748.
- (61) Li, H. L.; Zhu, Y. C.; Avivi, S.; Palchik, O.; Xiong, J. P.; Koltypin, Y.; Palchik, V.; Gedanken, A. Sonochemical Process for the Preparation of Alpha-CuSe Nanocrystals and Flakes. *J. Mater. Chem.* **2002**, *12*, 3723–3727.
- (62) Roy, P.; Srivastava, S. K. Nanostructured Copper Sulfides: Synthesis, Properties and Applications. *CrystEngComm* **2015**, *17*, 7801–7815.
- (63) Shamraiz, U.; Hussain, R. A.; Badshah, A. Fabrication and Applications of Copper Sulfide (CuS) Nanostructures. *J. Solid State Chem.* **2016**, *238*, 25–40.
- (64) Lu, Q. Y.; Gao, F.; Zhao, D. Y. One-Step Synthesis and Assembly of Copper Sulfide Nanoparticles to Nanowires, Nanotubes, and Nanovesicles by a Simple Organic Amine-Assisted Hydrothermal Process. *Nano Lett.* **2002**, *2*, 725–728.
- (65) Gao, L.; Wang, E. B.; Lian, S. Y.; Kang, Z. H.; Lan, Y.; Wu, D. Microemulsion-Directed Synthesis of Different CuS Nanocrystals. *Solid State Commun.* **2004**, *130*, 309–312.
- (66) Puspitasari, I.; Gujar, T. P.; Jung, K.-D.; Joo, O.-S. Simple Chemical Preparation of CuS Nanowhiskers. *Mater. Sci. Eng., B* **2007**, *140*, 199–202.
- (67) Zhu, Y.; Guo, X.; Jin, J.; Shen, Y.; Guo, X.; Ding, W. Controllable Synthesis of CuS Nanotubes and Nanobelts Using Lyotropic Liquid Crystal Templates. *J. Mater. Sci.* **2007**, *42*, 1042–1045.
- (68) Feng, X.; Yongxiu, L.; Huibiao, L.; Yuliang, L.; Shuang, C.; Ning, W.; Li, J.; Xiaofeng, L.; Mingjian, Y. Controlled Growth and Field Emission Properties of CuS Nanowalls. *Nanotechnology* **2007**, *18*, 145706-1–145706-5.
- (69) Mao, G.; Dong, W.; Kurth, D. G.; Möhwald, H. Synthesis of Copper Sulfide Nanorod Arrays on Molecular Templates. *Nano Lett.* **2004**, *4*, 249–252.
- (70) Chen, X.; Wang, Z.; Wang, X.; Zhang, R.; Liu, X.; Lin, W.; Qian, Y. Synthesis of Novel Copper Sulfide Hollow Spheres Generated from Copper (II)–Thiourea Complex. *J. Cryst. Growth* **2004**, *263*, 570–574.
- (71) Zou, J.; Zhang, J.; Zhang, B.; Zhao, P.; Xu, X.; Chen, J.; Huang, K. Synthesis and Characterization of Copper Sulfide Nanocrystal with Three-Dimensional Flower-Shape. *J. Mater. Sci.* **2007**, *42*, 9181–9186.
- (72) Zou, J.; Jiang, J.; Huang, L.; Jiang, H.; Huang, K. Synthesis, Characterization and Electrocatalytic Activity of Copper Sulfide Nanocrystals with Different Morphologies. *Solid State Sci.* **2011**, *13*, 1261–1267.
- (73) Liao, X.-H.; Chen, N.-Y.; Xu, S.; Yang, S.-B.; Zhu, J.-J. A Microwave Assisted Heating Method for the Preparation of Copper Sulfide Nanorods. *J. Cryst. Growth* **2003**, *252*, 593–598.
- (74) Lotfipour, M.; Machani, T.; Rossi, D. P.; Plass, K. E. Alpha-Chalcocite Nanoparticle Synthesis and Stability. *Chem. Mater.* **2011**, *23*, 3032–3038.
- (75) Kumar, P.; Gusain, M.; Nagarajan, R. Synthesis of Cu<sub>1.8</sub>S and CuS from Copper-Thiourea Containing Precursors; Anionic (Cl<sup>-</sup>, NO<sub>3</sub><sup>-</sup>, SO<sub>4</sub><sup>2-</sup>) Influence on the Product Stoichiometry. *Inorg. Chem.* **2011**, *50*, 3065–3070.
- (76) Wu, H. B.; Chen, W. Synthesis and Reaction Temperature-Tailored Self-Assembly of Copper Sulfide Nanoplates. *Nanoscale* **2011**, *3*, 5096–5102.
- (77) Lim, W. P.; Wong, C. T.; Ang, S. L.; Low, H. Y.; Chin, W. S. Phase-Selective Synthesis of Copper Sulfide Nanocrystals. *Chem. Mater.* **2006**, *18*, 6170–6177.
- (78) Du, X. S.; Mo, M. S.; Zheng, R. K.; Lim, S. H.; Meng, Y. Z.; Mai, Y. W. Shape-controlled Synthesis and Assembly of Copper Sulfide Nanoparticles. *Cryst. Growth Des.* **2008**, *8*, 2032–2035.
- (79) Reijnen, L.; Meester, B.; Goossens, A.; Schoonman, J. Chemical Vapor Deposition of Cu<sub>x</sub>S: Surface Contamination by Reaction Products. *Chem. Mater.* **2005**, *17*, 4142–4148.
- (80) Reijnen, L.; Meester, B.; de Lange, F.; Schoonman, J.; Goossens, A. Comparison of Cu<sub>x</sub>S Films Grown by Atomic Layer Deposition and Chemical Vapor Deposition. *Chem. Mater.* **2005**, *17*, 2724–2728.
- (81) Schneider, N.; Lincot, D.; Donsanti, F. Atomic Layer Deposition of Copper Sulfide Thin Films. *Thin Solid Films* **2016**, *600*, 103–108.
- (82) Xu, M.; Wu, H. Y.; Da, P. M.; Zhao, D. Y.; Zheng, G. F. Unconventional 0-, 1-, and 2-Dimensional Single-Crystalline Copper Sulfide Nanostructures. *Nanoscale* **2012**, *4*, 1794–1799.
- (83) Bryks, W.; Lupi, E.; Ngo, C.; Tao, A. R. Digenite Nanosheets Synthesized by Thermolysis of Layered Copper-Alkanethiolate Frameworks. *J. Am. Chem. Soc.* **2016**, *138*, 13717–13725.
- (84) Nessim, G. D.; Seita, M.; O'Brien, K. P.; Hart, A. J.; Bonaparte, R. K.; Mitchell, R. R.; Thompson, C. V. Low Temperature Synthesis of Vertically Aligned Carbon Nanotubes with Electrical Contact to Metallic Substrates Enabled by Thermal Decomposition of the Carbon Feedstock. *Nano Lett.* **2009**, *9*, 3398–3405.
- (85) Kronik, L.; Shapira, Y. Surface Photovoltage Spectroscopy of Semiconductor Structures: at the Crossroads of Physics, Chemistry and Electrical Engineering. *Surf. Interface Anal.* **2001**, *31*, 954–965.
- (86) Keenan, W. A.; Schneider, C. P.; Pillus, C. A. Type-All System for Determining Semiconductor Conductivity Type. *Solid State Technology* **1971**, *14*, 51–56.
- (87) Schroder, D. K.; *Semiconductor Material and Device Characterization*, 3rd ed.; John Wiley & Sons: Hoboken, NJ, 2006; p 7.
- (88) Momma, K.; Izumi, F. VESTA 3 for Three-Dimensional Visualization of Crystal, Volumetric and Morphology Data. *J. Appl. Crystallogr.* **2011**, *44*, 1272–1276.
- (89) Takano, Y.; Uchiyama, N.; Ogawa, S.; Mori, N.; Kimishima, Y.; Arisawa, S.; Ishii, A.; Hatano, T.; Togano, K. Superconducting Properties of CuS<sub>2-x</sub>Se<sub>x</sub> under High Pressure. *Phys. C* **2000**, *341*, 739–740.
- (90) Peng, Z.; Li, S.; Weng, M.; Zhang, M.; Xin, C.; Du, Z.; Zheng, J.; Pan, F. First-Principles Study of Cu<sub>9</sub>S<sub>8</sub>: A Novel p-Type Conductive Semiconductor. *J. Phys. Chem. C* **2017**, *121*, 23317–23323.
- (91) Fistul, V. I. *Heavily Doped Semiconductors*; Springer: New York, 1969.
- (92) Zhang, Y.; Wang, X.; Zheng, X.; Chen, G.; Ma, D.; Xu, F.; Thang, N.; Ge, W.; Shen, B. Effect of Grain Boundary Scattering on Electron Mobility of N-Polarity InN Films. *Appl. Phys. Express* **2013**, *6*, 021001-1–021001-3.
- (93) Cermak, J.; Yamada, T.; Ledinsky, M.; Hasegawa, M.; Rezek, B. Microscopically Inhomogeneous Electronic and Material Properties

Arising During Thermal and Plasma CVD of Graphene. *J. Mater. Chem. C* **2014**, *2*, 8939–8948.

(94) Nguyen, E. P.; Carey, B. J.; Daeneke, T.; Ou, J. Z.; Latham, K.; Zhuiykov, S.; Kalantar-zadeh, K. Investigation of Two-Solvent Grinding-Assisted Liquid Phase Exfoliation of Layered MoS<sub>2</sub>. *Chem. Mater.* **2015**, *27*, 53–59.

(95) Nguyen, E. P.; Carey, B. J.; Ou, J. Z.; van Embden, J.; Della Gaspera, E.; Chrimes, A. F.; Spencer, M. J. S.; Zhuiykov, S.; Kalantar-zadeh, K.; Daeneke, T. Electronic Tuning of 2D MoS<sub>2</sub> through Surface Functionalization. *Adv. Mater.* **2015**, *27*, 6225–6229.

(96) Song, X. X.; Hui, F.; Gilmore, K.; Wang, B. R.; Jing, G. Y.; Fan, Z. C.; Grustan-Gutierrez, E.; Shi, Y. Y.; Lombardi, L.; Hodge, S. A.; Ferrarie, A. C.; Lanza, M. Enhanced Piezoelectric Effect at the Edges of Stepped Molybdenum Disulfide Nanosheets. *Nanoscale* **2017**, *9*, 6237–6245.

(97) Duffy, R.; Foley, P.; Filippone, B.; Mirabelli, G.; O'Connell, D.; Sheehan, B.; Carolan, P.; Schmidt, M.; Cherkaoui, K.; Gatensby, R.; Hallam, T.; Duesberg, G.; Crupi, F.; Nagle, R.; Hurley, P. K. Structural and Electrical Investigation of MoS<sub>2</sub> Thin Films Formed by Thermal Assisted Conversion of Mo Metal. *ECS J. Solid State Sci. Technol.* **2016**, *5*, Q3016–Q3020.

(98) Boyle, J. J.; Giancoli, D. C. *Study guide: Physics: principles with applications*, 4th ed.; Englewood Cliffs: Prentice Hall, NJ, 1995.